



## Biotic induction and microbial ecological dynamics of Oceanic Anoxic Event 2

Gregory T. Connock <sup>1</sup>✉, Jeremy D. Owens<sup>2</sup> & Xiao-Lei Liu <sup>1</sup>

Understanding the causal mechanisms of past marine deoxygenation is critical to predicting the long-term Earth systems response to climate change. However, the processes and events preceding widespread carbon burial coincident with oceanic anoxic events remain poorly constrained. Here, we report a comprehensive biomarker inventory enveloping Oceanic Anoxic Event 2 that captures microbial communities spanning epipelagic to benthic environments in the southern proto-North Atlantic Ocean. We identify an abrupt, sustained increase in primary productivity that predates Oceanic Anoxic Event 2 by  $\sim 220 \pm 4$  thousand years, well before other geochemical proxies register biogeochemical perturbations. During the event, recurrent photic zone euxinia triggered a major marine microbial reorganization accompanied by a decrease in primary production. These findings highlight how organic carbon burial drivers operated along a continuum in concert with microbial ecological changes, with antecedent, localized increases in primary production destabilizing carbon cycling and promoting the progressive marine deoxygenation leading to Oceanic Anoxic Event 2.

<sup>1</sup>School of Geosciences, University of Oklahoma, Norman, OK 73019, USA. <sup>2</sup>Department of Earth, Ocean, and Atmospheric Science, Florida State University, and National High Magnetic Field Laboratory, Tallahassee, FL 32306, USA. ✉email: [gtconnock@gmail.com](mailto:gtconnock@gmail.com)

Global climate change, exacerbated by societal demands contributing to a sustained atmospheric CO<sub>2</sub> rise, is a widely accepted phenomenon affecting modern Earth. Anticipatory efforts seeking to characterize the oceanographic response to natural and anthropogenic forcings may benefit from an improved understanding of analogous periods in Earth history. Oceanic anoxic events (OAEs<sup>1</sup>) are oft-employed models of future climate, given the frequently associated high pCO<sub>2</sub><sup>2</sup> (and references therein) and temperatures<sup>3–5</sup> (and references therein) that facilitated the development of expansive marine deoxygenation in the past<sup>6,7</sup>.

Oceanic anoxic event 2 (OAE-2) is the most well-studied and widely observed OAE, as defined by a global positive carbon isotope excursion (+CIE) immediately prior to the Cenomanian-Turonian boundary (~93.9 Ma<sup>8,9</sup>). The +CIE, observed in both organic and inorganic carbon reservoirs, represents a major perturbation to the global biogeochemical carbon cycle whereby enhanced productivity and/or preservation led to a substantial fractional increase in organic carbon burial<sup>8,10</sup>. However, the causal mechanisms initiating and sustaining rampant deoxygenation of the marine realm remain poorly constrained. Recent investigations revealed progressive deoxygenation, potentially associated with large igneous province (LIP) activity, preceded OAE-2<sup>7,11</sup>. Yet direct evidence of heightened primary productivity, a mechanism producing progressive deoxygenation via organic carbon remineralization, prior to OAE-2 is lacking.

Biomarkers, molecular fossils of past microbial life, possess the potential to unravel the microbial ecological response bounding the OAE-2 interval. Previous biomarker studies provided critical insight into OAE-2, such as the spatiotemporal extents of photic zone euxinia<sup>12,13</sup> (PZE), and primary producer composition<sup>6,14–16</sup>, as well as estimates of sea surface temperature<sup>3,4</sup> and pCO<sub>2</sub><sup>2</sup> (and references therein), but all primarily reflect surface ocean processes which inherently limited paleoenvironmental reconstructions. Likewise, organic geochemical surveys of the Demerara Rise (~375 km north of Suriname) have been limited in scope, unable to capitalize on the continuous and exceptionally preserved<sup>17</sup> record enveloping OAE-2 due to deposition in relatively persistent reducing bottom waters<sup>6</sup>. Coarse sampling<sup>6,12</sup>, the narrow analytical window of GC-MS (gas chromatography-mass spectrometry) limiting interpretations to relatively nondescript biomarkers<sup>6,12,13</sup>, and a singular focus restricted to a specific biomarker class representative of only a portion of the water column (e.g., porphyrins or archaeal lipids<sup>4,16</sup>) has precluded a comprehensive understanding of the potential process(es) influencing microbial communities, and by extension, proxies reliant on specific biomarker distributions (e.g., TEX<sub>86</sub>-derived sea surface temperature). Thus, the impact of dynamic climatic states on the total marine microbial ecology requires clarification that is critical for interpretations of OAE-2 and subsequent application to modern climate change.

Here, we present an extensive biomarker inventory capturing the temporal evolution of microbial communities spanning the entire marine water column (i.e., surface to sediment). This new record and holistic approach allow us to leverage marine microbial variations to clarify the biotic response to and [potential] function in progressive deoxygenation antecedent to OAE-2, as well as to characterize the microbial ecological reorganization during, and recovery after, the event.

## Results

**Biomarker inventory.** Biomarkers were analyzed via liquid chromatography quadrupole time-of-flight mass spectrometry (LC-qTOF-MS) in 43 samples over a ~10 m depth transect of pre-OAE, OAE, and post-OAE strata at ODP Site 1258 on the

Demerara Rise (Fig. S1; see Site description and novelty in Supplementary Information). A diverse molecular fossil record was uncovered (Fig. 1; Supplementary Data 1), comprising cyclic tetrapyrroles (herein referred to as ‘tetrapyrroles’, including free-base chlorins, porphyrins, and metalloporphyrins; Supplementary Data 2), isorenieratane, dialkyl glycerol ethers (DAGEs), extended archaeols (C<sub>20/25</sub>, C<sub>20/30</sub>, C<sub>20/35</sub>), butanetriol/pentanetriol dialkyl glycerol tetraethers (BDGT/PDGT), and glycerol dialkyl glycerol tetraethers (GDGTs), including isoprenoidal GDGTs (isoGDGTs, such as crenarchaeol), branched GDGTs (brGDGTs), and overly-branched GDGTs (obGDGTs; see Fig. S2 for biomarker identifications).

Microbial ecological reconstruction of the epipelagic to benthic realms was possible given the relatively depth-specific biological origins of individual biomarkers (Fig. 2). Generalized residence depth, based on the habitats of the presumed source organisms, was used to categorize biomarkers for ease of discussion and is not necessarily definitive, with interpretations reliant on the paleoenvironmental implications of biomarker occurrences and distributions. ‘Shallow’ (epipelagic) refers to the tetrapyrroles, ‘intermediate’ (mesopelagic) to crenarchaeol, isorenieratane, and obGDGTs, and ‘deep’ (bathypelagic to benthic) to DAGEs, extended archaeols, and BDGT/PDGT. Tetrapyrroles, derived from chlorophylls present in photoautotrophs<sup>17,18</sup>, record depths extending from the sea surface to the top of the chemocline or base of the euphotic zone. Crenarchaeol, produced by the ammonia-oxidizing archaea *Thaumarchaeota*<sup>19,20</sup>, primarily monitors the zone immediately above the chemocline or below the base of the photic zone. Isorenieratane, a degradation product of isorenieratene biosynthesized predominantly by the anoxygenic photosynthetic sulfur-oxidizing bacteria *Chlorobiaceae*<sup>21</sup>, reflects the relative depth of the chemocline within the photic zone<sup>22</sup>. The development of an oxygen minimum zone (OMZ) or expanded bottom water anoxia is captured by the obGDGTs, sourced from unidentified anaerobic bacteria within or below the chemocline<sup>23</sup>. At greater depths beyond the photic zone and extending into the sediments, DAGEs<sup>24</sup>, extended archaeols<sup>25</sup>, and BDGT/PDGT<sup>26</sup> track deep water microbial compositions of sulfate-reducing bacteria, halophilic archaea, and methanogenic archaea, respectively. Interpretative confidence of microbial communities was greatest in well-established biomarkers comprising shallow and intermediate depths, whereas the novelty of biomarkers tracking bathypelagic and/or benthic organisms warranted inferential caution given the potential source(s) have not been extensively investigated and concentrations may be altered by post-depositional microbial activity, albeit unlikely (see Site description and novelty and Potential source(s) of deep (bathypelagic to benthic) biomarkers in Supplementary Information for further details). However, integration of the biomarker record with additional, published proxy data from the Demerara Rise (e.g., isotopes) helped minimize potential misinterpretation of the indigenous microbial signal and substantiate paleoenvironmental reconstructions.

Principal component analysis (PCA) highlighted the utility of our biomarker inventory to discern differences imposed by contrasting biogeochemical regimes. Biomarkers derived from intermediate and deep waters were most effective at differentiating OAE from non-OAE strata (Fig. S3). Tetrapyrroles were the predominant biomarker class across the studied interval, followed by crenarchaeol and isorenieratane. A sharp drop in tetrapyrrole fractional abundance, primarily due to an increase in isorenieratane concentrations, occurred immediately before the +CIE and was sustained through OAE-2 (Fig. 3). Other features defining OAE-2 include relatively low, invariant tetrapyrrole and crenarchaeol concentrations accompanied by elevated amounts of isorenieratane, obGDGTs, DAGEs, and extended archaeols (Fig. 4,

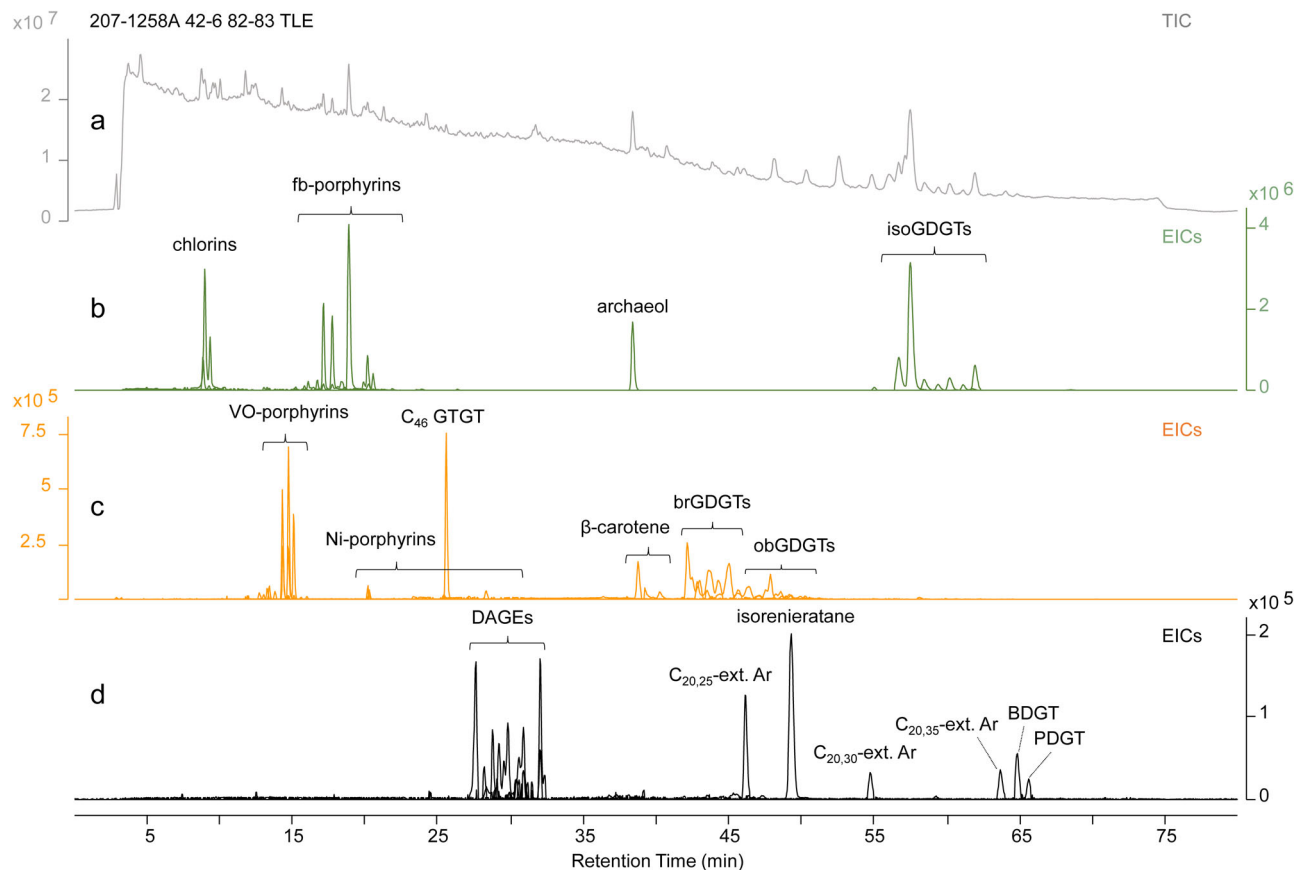


**Fig. 1 Total ion chromatogram (TIC) and summed extracted ion chromatograms (EIC) from LC-qTOF-MS analysis for sample 1258A 42-6 82-83.** **a** TIC depicting the overall signal intensity of major biomarkers and background metrics. **b–d** Combined EICs based on the relative abundance of targeted biomarker classes to show compound separation and abundance. Extracted  $m/z$  values based on theoretical exact masses of adduct ions: chlorins (533.2547, 535.2704); fb-porphyrins (449.2700, 477.3013, 479.3169, 487.2856, 489.3013); VO-porphyrins (514.1932, 540.2089, 542.2245, 554.2245); Ni-porphyrins (451.1427, 479.1740, 491.1740, 505.1897, 533.2210, 543.2053, 545.2210); archaeol and extended archaeols (ext. Ar; 653.6812, 723.7589, 793.8371, 863.9154); iso-GDGTs (1292.2444, 1294.2600, 1296.2757, 1298.2914, 1300.3070, 1302.3227); br-GDGTs (1022.0097, 1036.0253, 1050.0410); ob-GDGTs (1064.0566, 1078.0723, 1092.0879, 1106.1036, 1120.1192, 1134.1349); isorenieratane (564.5503); DAGEs (513.5241, 527.5398, 541.5554); BDGT/PDGT (1316.3383, 1330.3540).

Fig. S3). The initial deposition of pre-OAE (429.91–427.63 mcd, meters composite depth) and post-OAE strata was relatively similar based on PCA results, biomarker profiles and fractional abundances, excluding a period from 421.19 to 421.04 mcd where an abrupt increase of isorenieratane was observed. Spikes in tetrapyrroles, crenarchaeol, obGDGTs, and DAGEs at 427.54 mcd defined the latter phase of the pre-OAE interval. The DAGEs declined rapidly, but a gradual decrease in the tetrapyrroles, crenarchaeol, and obGDGTs, punctuated by brief positive excursions, extended into OAE-2 as isorenieratane concentrations progressively rose (Fig. 4). These stratigraphic variations in biomarker concentrations chronicle a previously undocumented pre-OAE biotic event predating the +CIE commonly used to demarcate OAE-2 initiation.

## Discussion

**The biotic induction of OAE-2.** The rapid proliferation of select microbial communities at 427.54 mcd likely represents a pre-OAE biotic perturbation (pre-OAE BP) presaging the protracted period of widespread marine deoxygenation during OAE-2, and progressive deoxygenation predating the +CIE<sup>7</sup> (Fig. 4). At the beginning of the pre-OAE BP (427.54 mcd), abruptly elevated tetrapyrroles and crenarchaeol concentrations signify an abrupt increase in primary production by photoautotrophs and chemoautotrophs residing above the chemocline. Increased volumes

of precipitating biogenic snow concordantly consumed oxygen, expanding the preexisting OMZ as anaerobic bacteria thrived based on accelerated obGDGTs synthesis. Euxinia did not penetrate the photic zone at the outset of the productivity bloom as isorenieratane was not detected and heightened rates of microbial sulfate reduction were seemingly transient, inferred from the DAGEs profile, and limited to pre-OAE BP initiation. The lack of a well-stratified water column, evinced by absent to low concentrations of halophilic archaeal lipids (i.e., extended archaeols), relatively low rates of microbial sulfate reduction, and a dense oxygenic microbial plate likely precluded the development of PZE initially.

Establishing a definitive causal mechanism for the pre-OAE BP is difficult, but the concomitance of LIP activity with the productivity spike is intriguing. Application of a linear sedimentation rate from OAE-2 to the pre-OAE BP interval following previous works<sup>6,7</sup> approximated the pre-OAE BP occurring  $220 \pm 4$  kyr before OAE-2, lasting for  $\sim 100$  kyr (427.54–426.88 mcd; see Estimating the duration of the pre-OAE BP in Supplementary Information for rationale and calculation). Significantly, this was roughly coincident with the onset of LIP activity ( $\sim 200$ – $300$  kyr before OAE-2) inferred from marine osmium isotope stratigraphy<sup>27</sup>. Similarities in the modern planktonic community response, such as elevated productivity and compositional changes, between the 2018 Kilauea eruption<sup>28</sup> and the pre-OAE BP reinforce inference of a potential

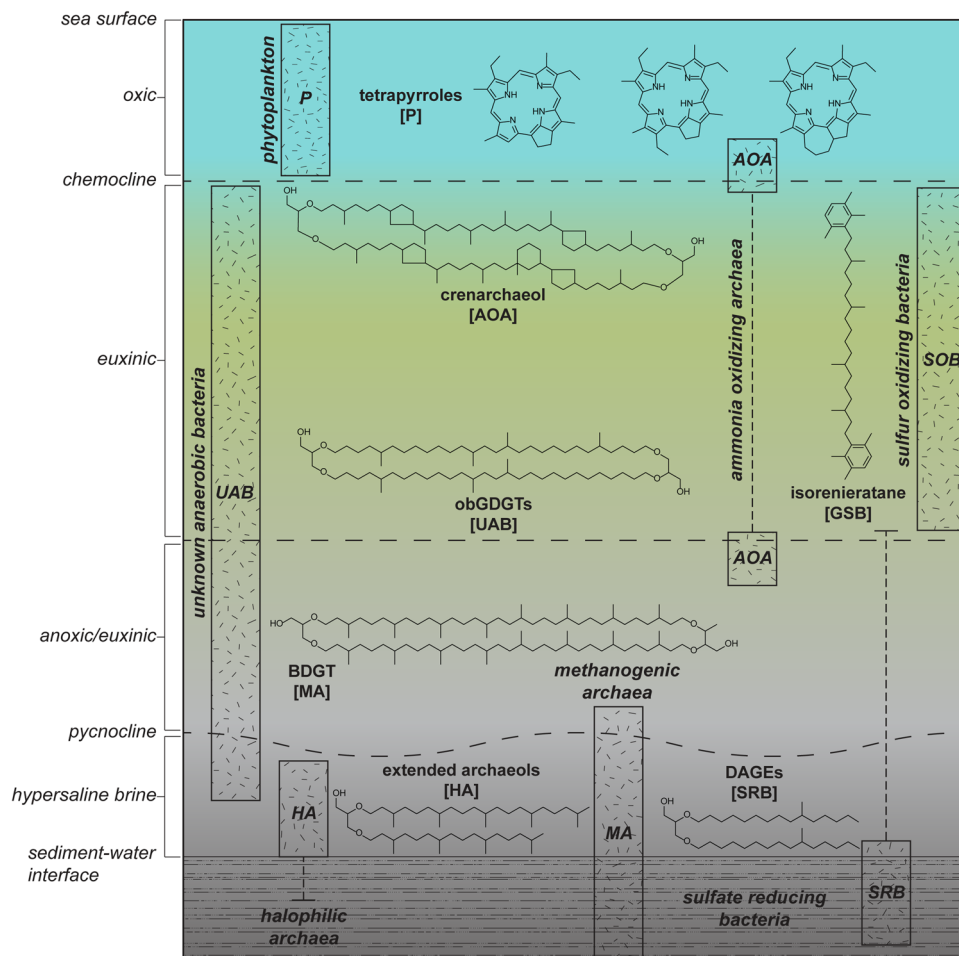


**Fig. 2** An idealized 2-D water column portraying the depth distribution and source organisms of biomarkers detected in mid-Cretaceous strata from Site 1258, Demerara Rise. The residence depths of specific microbes are illustrated using rectangles, spanning habitable depth ranges, and containing relevant abbreviations (e.g., sulfur-oxidizing bacteria = SOB). Vertical hashed lines represent regions potentially occupied by a specific organism but beyond their ideal depth range. Selected biomarker structures are depicted to portray the compound diversity hosted in sediments from the Demerara Rise, with the source organism abbreviation in brackets.

magmatic trigger for this event (see Evidence for LIP trigger of the pre-OAE biotic perturbation in Supplementary Information for additional details).

A constant, yet overall lower, nutrient and trace metal inventory<sup>6</sup> (Fig. S4) combined with a redox-driven shift in fixed N species (from  $\text{NO}_3^-$  to  $\text{NH}_4^+$ )<sup>15</sup>, potentially leading to a fixed N shortage<sup>29</sup> via intensified denitrification and anammox reactions<sup>30</sup>, were probable culprits in the failure to sustain prolific rates of primary production beyond 100 kyr at the Demerara Rise. The gradual decline in biomass production, indicated by decreasing tetrapyrrole and crenarchaeol profiles (Fig. 4), was accompanied by a notable shift in deep water communities. Sulfate-reducing bacteria exerted increasing predominance over methanogenic archaea, a trend coeval with the primary productivity spike and extending well into the OAE (Fig. 3). A collapse of autotrophic communities to pre-perturbation levels was concordant with the progressive shoaling of  $\text{H}_2\text{S}$ -laden waters. Continued vertical migration of the chemocline intruded the photic zone, producing PZE that enabled anoxygenic photosynthesis by *Chlorobiaceae* (Fig. 4). Unlike the overall oscillatory character of PZE throughout the studied section, this protracted phase of PZE was sustained until the onset of OAE-2 (426.43–426.00 mcd, Figs. 3 and 4) and is approximately contemporaneous with a thallium (Tl) isotope excursion<sup>7</sup> (426.40–426.30 mcd).

The positive Tl isotope excursion represents the progressive expansion of bottom water anoxia predating OAE-2 by  $43 \pm 11$  kyr<sup>6,7</sup>. However, evidence for a causal mechanism of pre-OAE deoxygenation remains indeterminate. Our comprehensive biomarker inventory provides an interpreted sequence of events culminating in the regional to global expansion of anoxia predating OAE-2. A protracted phase of enhanced primary productivity began  $\sim 220 \pm 4$  kyr prior to OAE-2, increasing localized production and export of organic carbon at Demerara Rise. Similar productivity spikes likely occurred in settings of comparable paleogeographic configuration (e.g., equatorial, continental margins/shelves), seeding the oceans with fixed carbon. Continued scavenging of marine oxygen via organic carbon remineralization resulted in OMZ expansion locally, and likely initiated oxygen drawdown in much of the proto-North Atlantic Ocean. Stratigraphic records of sulfur isotopes of pyrite ( $\delta^{34}\text{S}_{\text{pyrite}}$ ) from the proto-North Atlantic and Tethys Oceans<sup>11</sup> validate the areal extrapolation of our interpretations. A gradual decline in  $\delta^{34}\text{S}_{\text{pyrite}}$  values at Demerara Rise begins at 427.50 mcd, nearly identical to the onset of the pre-OAE BP (427.54 mcd, Fig. 4). Correlation of  $\delta^{34}\text{S}_{\text{pyrite}}$  in a global transect (Western Interior Seaway, proto-North Atlantic, Tethys) revealed consistent behavior in  $\delta^{34}\text{S}_{\text{pyrite}}$  prior to the +CIE, indicating increasingly expansive marine deoxygenation on a global scale<sup>11</sup>. Over  $\sim 100$  kyr, increased regional biomass production induced

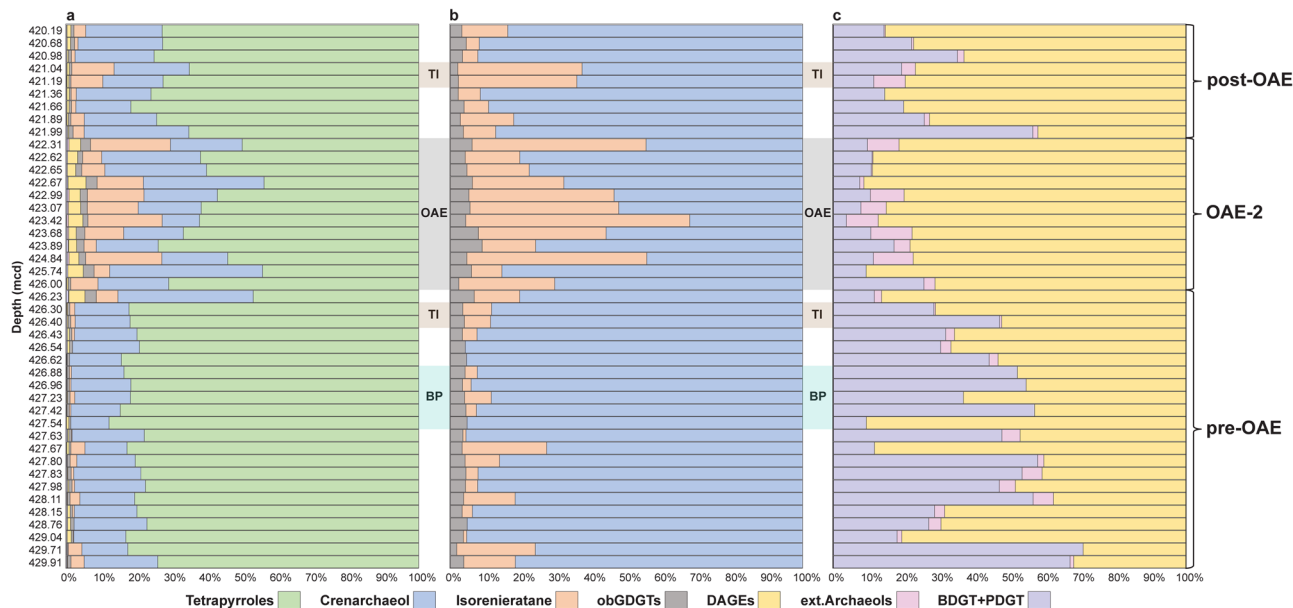


**Fig. 3 Biomarker fractional abundances preceding, during, and following OAE-2.** **a** The fractional abundance of individual biomarkers, representative of the entire water column. **b** The fractional abundance of biomarkers derived exclusively from intermediate depths. **c** The fractional abundance of lipids produced by deep water microbial communities. The color-shaded intervals represent the timing and duration of the pre-OAE biotic perturbation (BP), thallium isotope excursions (TI), and OAE-2 (OAE).

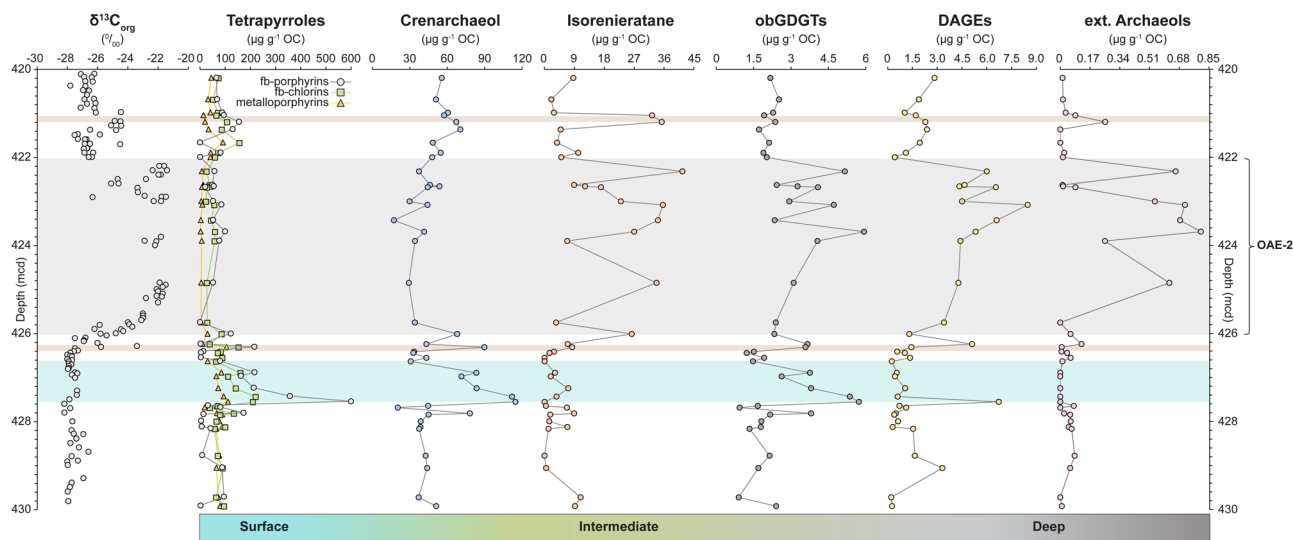


**Fig. 4 Depth profiles of biomarkers through the studied section.** Biomarkers are ordered from left to right by increasing residence depth, indicated by the shaded rectangle and associated labels ‘Surface’, ‘Intermediate’, and ‘Deep’. The blue shaded interval represents the pre-OAE biotic perturbation, the gray shaded interval represents OAE-2, and the brown shaded intervals represent the positive TI isotopic excursions. Stable organic carbon isotopic data of the studied core interval, derived from previous works<sup>6,9</sup>, is shown for reference. The tetrapyrroles are comprised of three individual logs, the free-base porphyrins (fb-porphyrins), free-base chlorins (fb-chlorins), and summed VO-, Ni-, Fe-, and Zn-metalloporphyrins. The obGDGTs, DAGEs, extended archaeols, and individual tetrapyrrole profiles are comprised of multiple compounds (see Supplementary Information for additional details).

pervasive marine anoxia, inhibiting Mn-oxide formation, producing the observed positive TI isotope excursion, and ultimately, the globally observed +CIE reflecting enhanced organic carbon burial signaling the onset of OAE-2. Thus, the local biotic signal recorded at ODP Site 1258 underlines the crucial role the Demerara Rise, and similar undocumented settings, served in initiating deoxygenation of the global ocean.

**Microbial ecological dynamics during and after OAE-2.** Changes in microbial community compositions during OAE-2 were apparent, signified by a shift in the normalized total

biomarker pool (Fig. 3) and variations in the absolute concentrations of individual biomarkers (Fig. 4). In general, OAE-2 was defined by an expansion and diversification of intermediate and deep water communities (426.00–423.07 mcd), followed by a period of instability leading to the termination of the OAE (423.07–422.00 mcd). Photo- and chemoautotrophs residing above the chemocline were adversely affected, evinced by relatively low, invariant tetrapyrrole and crenarchaeol profiles (Fig. 4). Based on these observations, we divided OAE-2 into two periods defined by contrasting paleoenvironmental conditions modulating the microbial inhabitants of Demerara Rise.

The first period of OAE-2 (426.00–423.07 mcd, Fig. 4) was marked by the intrusion of a euxinic OMZ into the photic zone. Elevated, yet fluctuating isorenieratane concentrations suggest relatively persistent PZE of varying vertical extent, in agreement with previous investigations using biomarkers and nitrogen isotopes at nearby sites<sup>12,13,31</sup>. During this interval, microbial sulfate reduction was likely active as DAGEs continually increased, aligning with estimates of expanded seafloor euxinia<sup>32</sup>. The co-occurrence of abundant extended archaeols and isorenieratane intimates the role that density stratification served in maintaining the protracted PZE of OAE-2, substantiating concurrent findings based on neodymium<sup>33</sup> and oxygen isotopes<sup>34</sup>. Vertical nutrient advection via upwelling<sup>35</sup> led to preferential exposure to expanding intermediate water communities tolerant to sulfidic conditions in the OMZ. Scavenging of a potentially limited fixed N inventory<sup>30</sup>, depleted in  $\text{NO}_3^-$  and predominated by  $\text{NH}_4^+$ <sup>15,29</sup>, and inhibition of efficient nutrient transfer by pronounced density stratification likely induced severe N deficiency in surface water communities, explaining the relatively muted productivity of oxygenic photoautotrophs (i.e., tetrapyrroles) and chemoautotrophs (i.e., crenarchaeol) observed (Fig. 4). The concentration and predominant utilization of fixed N in the OMZ led to the proliferation and diversification of intermediate and deep water microbial taxa, while a shoaling chemocline led to increased nutrient (i.e., fixed N) competition between photoautotrophs and retreating *Thaumarchaeota* as highlighted by our biomarker inventory and the nitrogen isotopic record<sup>31</sup>. These findings challenge previous interpretations of highly productive, predominantly eukaryotic primary producers reliant on the upwelling of isotopically depleted  $\text{NH}_4^+$  during OAE-2<sup>15</sup>. Instead, the decline of  $\text{C}_{30-17}\text{-nor-DPEP}$  (Fig. S5; Supplementary Data 3), a source-specific tetrapyrrole diagenetically derived from algal chlorophyll-*c*<sup>36</sup>, and reconstructed water column conditions during OAE-2 indirectly support a rise in cyanobacteria, diazotrophs able to fix  $\text{N}_2$ , in oxygenated, nutrient-depleted shallow waters. Increased cyanobacterial contribution is further supported by C and N stable isotopes<sup>16,37</sup>, as well as the prominence of potentially phylum-specific biomarkers across OAE-2 (e.g., 2-methylhopanoids<sup>6,14</sup>).

A reversal from the formerly outlined conditions typified the second period of OAE-2 (423.07–421.99 mcd, Fig. 4). Destabilization of the stratified water column and reduced production of  $\text{H}_2\text{S}$  led to deepening and contraction of the euxinic OMZ. The observed decline in halophilic archaea, coincident with an overall decline in *Chlorobiaceae* populations, is roughly coeval with positive neodymium isotopic excursions observed across the proto-North Atlantic<sup>33</sup> attributed to the enhanced latitudinal commingling of proto-North Atlantic water masses<sup>38</sup>. Although detrimental to sustained PZE, the persistence of a well-developed anaerobic bacterial community (i.e., obGDGTs) suggests the lasting presence of a non-euxinic OMZ despite improved bottom water circulation. A premature recovery of the chemoautotrophic *Thaumarchaeota*, inhabiting the base of the photic zone, relative to the shallower dwelling obligately oxygenic phototrophs (Fig. 3) likely reflects reduced toxicity associated with retreating euxinic waters, lessened resource competition with [primarily] *Chlorobiaceae*, and a competitive advantage tied to preferential exposure to upwelled nutrients and tolerance to low  $\text{O}_2$  conditions.

The termination of OAE-2 was marked by the temporary re-establishment of microbial community compositions mirroring those observed prior to the pre-OAE BP (Figs. 3 and 4). Contraction of the OMZ led to a deep chemocline, with PZE restricted to the basal photic zone as the production of reduced sulfide species diminished. The *Thaumarchaeota* continued the recovery initiated towards the latter half of OAE-2, accompanied by the rebounding oxygenic photoautotrophs. However, the

recovery of shallow autotrophic communities was halted by an episode of PZE (421.19–421.04 mcd) based on abrupt increases in isorenieratane concentrations (Fig. 4). Temporary development of pronounced density stratification likely facilitated the accumulation of  $\text{H}_2\text{S}$  in the lower to intermediate photic zone, producing the short-lived PZE episode. Interestingly, covariant responses observed in additional biomarker profiles (e.g., obGDGTs) to PZE during OAE-2 were not evident across this post-OAE interval, possibly due to the transient nature of PZE at this time. For example, the initial increase in isorenieratane concentrations at the onset of OAE-2 was not immediately accompanied by shifts in other biomarker classes (e.g., obGDGTs; Fig. 4), suggesting frequent recurrences of PZE may be required to illicit a major microbial ecological response as observed later during the OAE. Still, this brief episode of post-OAE PZE (421.19–421.04 mcd) coincides with a positive organic carbon isotope excursion<sup>9</sup> (Fig. S5), trace metal drawdown<sup>6</sup> (Fig. S4), and minor positive Tl isotope excursion<sup>7</sup> at the Demerara Rise. Prior study<sup>7</sup> tentatively attributed this interval to enhanced carbon burial during a post-OAE deoxygenation event of smaller magnitude, with subsequent work revealing continued pyrite burial post-OAE 2<sup>11</sup>. Our biomarker inventory revealed some environmental consistencies (e.g., PZE) between this interval and OAE-2, but the overall biotic response to this post-OAE geochemical perturbation was relatively subdued and requires additional sampling and investigation to properly constrain.

**Broader implications.** The recognition of the pre-OAE BP and evolving water column conditions at Demerara Rise highlights additional complexities of a dynamic ocean relevant to interpretations of OAE-2 and the +CIE. Enhanced, sustained, and widespread carbon burial is required to produce the +CIE used to define OAE-2<sup>8,10</sup>. Still, the principal forcing, productivity or preservation, remains enigmatic as evidence for the former mounts<sup>12,39</sup>.

Based on the tetrapyrrole profiles (Fig. 4) primary production was greatest during the pre-OAE BP and relatively muted throughout OAE-2 at Demerara Rise, assuming minimal alteration to the genetic tetrapyrrole stratigraphic signal. Biomass preservation was presumed enhanced during OAE-2 through sulfurization<sup>11</sup>, as the OMZ transitioned from anoxic to euxinic and penetrated the photic zone, yet low tetrapyrrole concentrations persist. Previous work noted a similar discrepancy between preservation potential and porphyrin abundance, postulating a paucity of trace metals to chelate with the free-base porphyrins induced poor preservation as desulfurization did not reveal additional porphyrin content<sup>16</sup>. However, both the pre-OAE BP and OAE-2 were characterized by relatively depleted trace metal inventories<sup>6</sup> (Fig. S4), yet exhibit contrasting tetrapyrrole profiles, suggesting relative changes in primary production were the predominate control on the stratigraphic distribution of tetrapyrroles across the studied interval at the Demerara Rise. The strong covariance between tetrapyrrole and crenarchaeol concentrations reinforces the interpretation tetrapyrroles faithfully reflect primary production (Fig. S6). Crenarchaeol, a biosynthetic product of chemoautotrophic archaea (*Thaumarchaeota*) comprising up to 20% of all archaea and bacteria in the modern ocean<sup>40</sup>, is structurally distinct from the tetrapyrroles making it likely that diagenetic alteration of the two biomarkers is not consistent in rate or form. Thus, the positive correlation between key proxies for major contributors to primary production, the photoautotrophs and chemoautotrophs, minimizes concern for the integrity of the biotic signal at Demerara Rise (see Tetrapyrroles as a record of primary production in Supplementary Information for additional details).

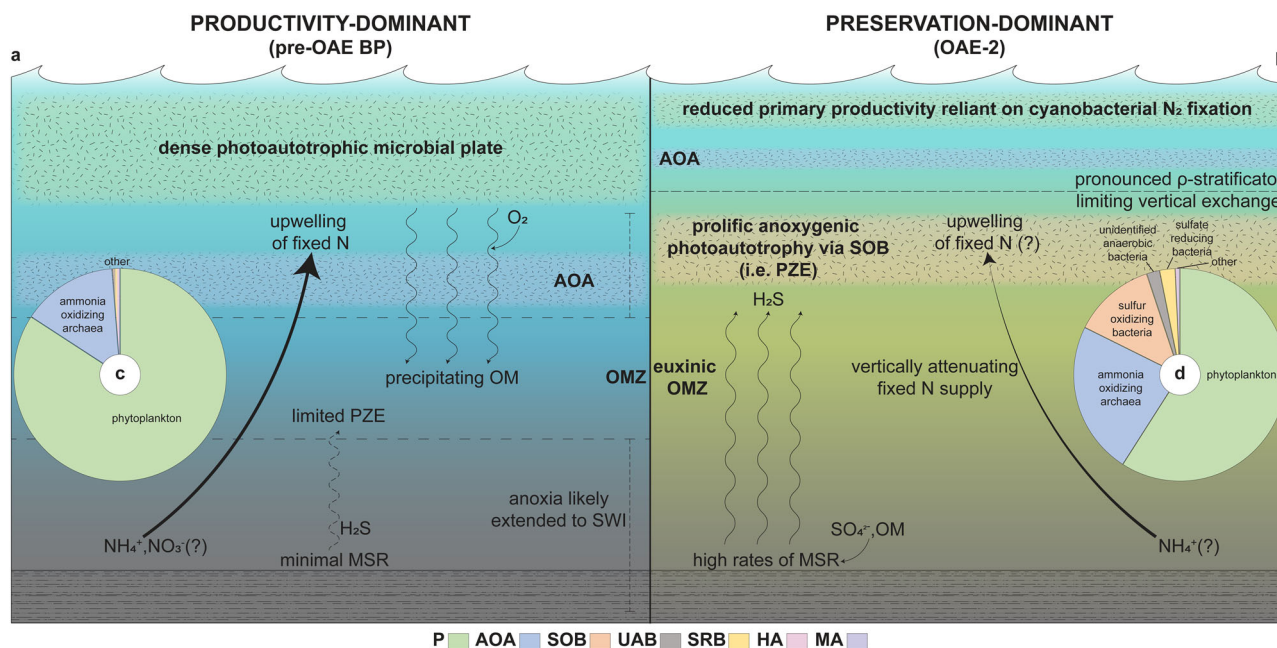


**Fig. 5** Contrasting biogeochemical conditions between the pre-OAE BP and OAE-2. **a, b** Microbial ecology and water column conditions during the pre-OAE BP, reflecting high primary production of organic carbon (**a**) and OAE-2, characterized by relatively lower organic carbon production, but substantially enhanced biomass preservation (**b**). **c, d** Averaged fractional abundances of individual biomarkers throughout the pre-OAE BP (**c**) and OAE-2 (**d**). Biomarker source organisms are abbreviated as follows: phytoplankton (P), ammonia oxidizing archaea (AOA), sulfur oxidizing bacteria (SOB), unknown anaerobic bacteria (UAB), sulfate reducing bacteria (SRB), halophilic archaea (HA), methanogenic archaea (MA).

These findings provide direct evidence for a causal mechanism resulting in both the Tl isotope excursion and +CIE as previously described. It is highly probable the pre-OAE BP was not exclusive to the Demerara Rise based on the immense and presently unconstrained organic carbon burial required to produce the +CIE<sup>10</sup>. Further characterization of comparable localities to Demerara Rise may reveal similar high productivity events, as primed, highly productive settings likely capitalized on exogenous nutrient delivery via efficient upwelling to the photic zone prior to stratification during OAE-2. Hence, OAE-2 and the +CIE were not coincident with heightened surface water productivity relative to the pre-OAE BP at the Demerara Rise. Rather, antecedent increases in primary production locally facilitated the initiation of the OAE as a mechanism to consume marine oxygen and subsequently enhance organic carbon preservation globally. This highlights how OAE-2, and perhaps other OAEs in the geologic record, were not instantaneously induced but rather a gradual transition stemming from sustained forcing(s). In addition, the occurrence of the pre-OAE BP well before the established onset of OAE-2 reveals how fluctuations in primary production can be linked to marine deoxygenation but may not necessarily be concurrent. As shown here, OAE-2 at the Demerara Rise was preceded by elevated primary production that progressively attenuated towards event onset. While the hallmark features of an OAE are well-established, further identification and refinement of trends preceding widespread anoxia in the past will improve our understanding of how marine deoxygenation develops, as well as our ability to assess planetary health today.

A shift from a productivity- to preservation-dominant system during OAE-2 at Demerara Rise, and possibly similar paleogeographic settings experiencing the pre-OAE BP, facilitated substantial organic carbon burial producing the +CIE. Distinct shifts in water column chemistry and structure from the pre-OAE BP to OAE-2 imparted considerable changes on microbial life, which altered the primary driver governing biomass sequestration (Fig. 5). Yet, both intervals reveal relatively comparable

carbonate-corrected total organic carbon values<sup>6</sup> (Fig. S5), signifying enhanced preservation as a critical component of organic carbon burial during OAE-2 at Demerara Rise. Consequently, this work suggests that sustained increases in primary production prior to OAE-2 initiated and regulated pre-OAE deoxygenation, resulting in a progressive shift to preservation as the primary control on organic carbon accumulation in sediments. Expanding euxinia and attendant changes to biogeochemical cycling adversely affected primary producers while simultaneously enhancing organic matter preservation via sulfurization<sup>11</sup>. Flourishment of *Thaumarchaeota* in oligotrophic settings in the modern open ocean<sup>41</sup>, and lack thereof during OAE-2 based on diminished crenarchaeol concentrations, underscores the scarcity of bioessential elements (e.g., fixed N) caused by microbial utilization of electron acceptors further down the redox ladder due to intensified marine anoxia, ultimately limiting primary production. The switch from a productivity to preservation model, reconstructed using biomarkers (Fig. 5) and initially suggested based on drawdown of the trace metal inventory<sup>6</sup>, was also concomitant with relative warming<sup>4</sup>. Simulated projections of the marine microbial response to continued global warming in the future revealed similar biotic trends (e.g., decreased primary productivity) to warming-induced oceanographic changes<sup>42</sup> (e.g., intensified stratification) observed during OAE-2. Thus, an abundance of proxy- and model-based results paired with conceptual evidence suggest relatively low production and enhanced preservation of organic carbon throughout OAE-2 at the equatorial Demerara Rise.

The pre-OAE BP may foreshadow greater regional trends observed during OAE-2. Equatorial upwelling centers, like Demerara Rise, are spatially restricted and represent regions of already high primary production before OAE-2. Climatic shifts concurrent with OAE-2 may have produced favorable conditions for elevated primary productivity in regions unable to capitalize on or exposed to allochthonous nutrient delivery prior to the +CIE. While the pre-OAE BP offers a causal mechanism for the

Tl isotope excursion and +CIE initiation, areal expansion of organic carbon preservation and production is necessary to sustain enhanced organic carbon burial for the duration of the +CIE.

Continued development of preexisting proxies is critical to extract and clarify current understandings of major climatic events in Earth history. Although reliant on excellent preservation of the microbial signal, the analytical and interpretative approach used here enables simultaneous examination of a wide array of biomarkers, producing a more holistic reconstruction of oceanographic changes inferred from microbial ecological variations spanning the surface to the sediment. This is timely, as investigations of the sedimentary archives become increasingly valuable analogs to understand the response of modern oceans to natural and anthropogenic forcings. Similarities between the pre-OAE BP and modern, climate-driven marine deoxygenation are concerning, while particular attention to preexisting highly productive settings may hold the key to forecasting the geologically rapid transition to a global OAE. Even though natural processes are currently beyond our control, stifling anthropogenic catalysts of climate change may decelerate the unfortunate, progressive suitability of OAEs as climate analogs in the future.

## Methods

**Sample preparation.** Forty-three composite core samples from ODP Leg 207 Site 1258 (cores A, B, and C, Demerara Rise) were provided in pre-cleaned micro-centrifuge tubes to the Geobiology Lab at the University of Oklahoma as powdered sample splits with methods for sample processing previously outlined<sup>6</sup>. For ease of communication, a visual is provided depicting the preparatory procedure (Fig. S7).

Approximately 150 mg of powdered core sample was transferred from the centrifuge tube to a glass 4 mL vial. Two internal standards, 100 ng of C<sub>46</sub> glycerol trialkyl glycerol tetraether (GTGT) and 1 µg of β-carotene, were introduced to the sediment powder for relative quantification of target compounds integrated from LC-qTOF-MS scans. A 1.5 mL 1:1 azeotrope of DCM:MeOH was added to the 4 mL vial, which was then vortexed prior to 20 min of ultrasonication for sample extraction. Post-sonication, samples were centrifuged at 3000 rpm for 5 min. The supernatant of each sample was transferred to a 2 mL vial and dried under a gentle stream of N<sub>2</sub>. The introduction of 1.5 mL of DCM:MeOH (1:1), sonication, centrifugation, transferring, and drying was repeated twice more for a total of three extractions. The final combined extract of each sample was blown to complete dryness and massed to yield quantitative results of the total lipid extract (TLE). The weighed TLE was brought up in 1 mL of 100% MeOH, ultrasonicated for 5 min, and centrifuged at 3000 rpm for 5 min. The supernatant was transferred to a new 2 mL vial for LC-qTOF-MS analysis.

**LC-qTOF-MS.** LC-MS was performed with an Agilent 1290 series UPLC system coupled to Agilent 6530 qTOF mass spectrometer through an Agilent jet stream dual electrospray ionization (AJS-ESI) interface. The ESI drying gas (N<sub>2</sub>) temperature was set at 300 °C, the N<sub>2</sub> flow rate was 8 L min<sup>-1</sup> and the nebulizer gas (N<sub>2</sub>) pressure was 35 psi. The qTOF parameters were set to: capillary voltage 3.5 kV, fragmentor voltage 175 V, skimmer voltage 65 V, and octupole voltage 750 V in auto MS/MS scanning mode with MS1 range of *m/z* 100–2000 and MS2 mass range of *m/z* 50–2000. Separation of compounds was achieved by dissolving the TLE in methanol and injecting 10 µL onto two Agilent Poroshell 120 EC-C18 columns (1.8 µm, 2.1 × 150 mm) in series maintained at 35 °C. The LC program was modified from a previously described reverse-phase LC method<sup>43</sup>. A flow rate of 0.2 mL min<sup>-1</sup>, first from 100% A to 90% A and 10% B in 5 min, was initially used and followed by a gradient to 35% B at 30 min, and to 50% B at 70 min, and finally re-equilibrated with 100% A for 10 min, where the eluent A was 95:5:0.04:0.10 of methanol/H<sub>2</sub>O/formic acid/14.8 M NH<sub>3</sub>(aq.) and B was 50:50:0.04:0.10 of hexane/2-propanol/formic acid/14.8 M NH<sub>3</sub>(aq.).

**Biomarker identification and quantification.** Biomarkers discussed in the text are identified based on accurate masses, chromatographic behavior (retention time compared with authentic standards), and characteristic fragmentation patterns of MS2. Extracted ion chromatograms (EICs) and representative molecular structures of major compounds as shown in Fig. 1 are presented in Fig. S2A–D. Hydroxychlorophyllones-a and meso-hydroxychlorophyllones-a are C<sub>33</sub> chlorins, each containing two isomer peaks (Fig. S2A), detected in all analyzed samples. The exceptional preservation of meso-hydroxychlorophyllones-a in Demerara Rise black shales has been previously documented<sup>17</sup>. Major free-based porphyrins include C<sub>33</sub> BiCAP, C<sub>32</sub> Etio, C<sub>32</sub> DPEP, and C<sub>30</sub> DPEP (Fig. S2A). Metalloporphyrins associated with vanadyl (VO), nickel (Ni), Zinc (Zn), and Iron (Fe) are

recognized in analyzed samples (Fig. S2B). VO<sup>2+</sup>, Ni<sup>2+</sup>, and Zn<sup>2+</sup> chelated to porphyrins are divalent, and these metalloporphyrins are detected as protonated ions, [M + H]<sup>+</sup>, but Fe-porphyrin occurs as M<sup>+</sup> due to the presence of trivalent metal ion, Fe<sup>3+</sup>. The specific C<sub>30</sub>-17-nor-DPEP, C<sub>30</sub>-VO-17-nor-DPEP, and C<sub>30</sub>-Ni-17-nor-DPEP are assigned to the latest isomer peak of C<sub>30</sub> DPEP, C<sub>30</sub>-VO-DPEP, and C<sub>30</sub>-Ni-DPEP based on the retention time of 17-nor-DPEP standards (generously provided by Dr. Kashiwama, see initial identification of 17-nor-DPEP<sup>36</sup>). Glycerol ether lipids (Fig. S2C and D) including the tetraethers (isoGDGTs, brGDGTs, obGDGTs, BDGT, and PDGT) and diethers (archaeol, extended archaeol, and DAGEs) are identified by their MS2 fingerprints reported in previous works<sup>21,44,45</sup>. OH-GDGT and S-GDGT were not discussed in the text but shown in Fig. S2C to illustrate the distinct retention time of isoGDGT-1. The soil-derived 5-methyl brGDGTs and aquatic bacterial 6- and 7-methyl brGDGTs isomers were distinguished by comparing results of a soil extract containing only the 5-methyl brGDGTs and a modern marine sediment sample with all isomers. The distribution of 7-methyl brGDGTs is not discussed in this work. Extended archaeols synthesized by cultured halophilic archaeal species are known to contain a phytane and a C<sub>25</sub> (C<sub>20,25</sub> ext. Ar), or two C<sub>25</sub> isoprenoids hydrocarbons (C<sub>25,25</sub> ext. Ar)<sup>46</sup>. Novel extended archaeol derivatives with up to C<sub>40</sub> isoprenoid are tentatively identified based on their MS2 in this study (Fig. S2D). The occurrence of isorenieratane in the Demerara Rise black shales is confirmed by MS2 and retention times of C<sub>40</sub> aromatic carotenoids previously identified in the Woodford Shale extracts<sup>47</sup>. β-carotene was used for the quantification of aromatic carotenoids, and C<sub>46</sub> GTGT for GDGTs. Due to the lack of authentic standards for all other compound classes, C<sub>46</sub> GTGT was used for their quantitative analysis. Considering potential quantitative bias caused by the response factors of different compound classes, discussions in text were restricted to relative variations within each compound class, and were not solely based on comparisons of absolute concentrations of different biomarkers. Comparisons of biomarker concentrations stemming from structurally distinct compound classes were conducted with caution, with interpretations only presented when substantiated by coincident stratigraphic trends and/or previously published supplemental proxy data. Critically, discussion of stratigraphic changes in the abundance of a specific biomarker class eliminates concern over contrasting ionization efficiencies since biomarkers of comparable molecular structure (e.g., tetrapyrroles) were normalized to the same internal standard. This approach provides insight into the relative temporal changes in biomarker concentrations related to microbial ecological changes, while the use of more structurally similar standards would only afford greater confidence on absolute concentrations not entirely relevant to aims of this work. However, efforts are currently underway to implement additional standards into the preparatory procedure to address the structural diversity uncovered by the LC-qTOF-MS method (see LC-qTOF-MS method reproducibility and detection limits in Supplementary Information for more details).

## Data availability

Data used in this study were generated via LC-qTOF-MS analysis of powdered core samples from Site 1258 on the Demerara Rise (ODP Leg 207) and are publicly available at pangaea.de (deposition title: LC-qTOF-MS biomarker data across the OAE-2 interval at the Demerara Rise; authors: Gregory T. Connock, Jeremy D. Owens, Xiao-Lei Liu).

Received: 16 March 2021; Accepted: 30 May 2022;

Published online: 16 June 2022

## References

- Schlanger, S. O. & Jenkyns, H. C. Cretaceous oceanic anoxic events: causes and consequences. *Geol. Mijnb.* **55**, 179–184 (1976).
- Witkowski, C. R., Weijers, J. W. H., Blais, B., Schouten, S. & Damsté, J. S. S. Molecular fossils from phytoplankton reveal secular *p*CO<sub>2</sub> trend over the Phanerozoic. *Sci. Adv.* **4**, eaat4556 (2018).
- Schouten, S., Hopmans, E. C., Schefuß, E. & Damsté, J. S. S. Distributional variations in marine crenarchaeotal membrane lipids: a new tool for reconstructing ancient sea water temperatures? *Earth Planet. Sci. Lett.* **204**, 265–274 (2002).
- Forster, A., Schouten, S., Moriya, K., Wilson, P. A. & Damsté, J. S. S. Tropical warming and intermittent cooling during the Cenomanian/Turonian oceanic anoxic event 2: Sea surface temperature records from the equatorial Atlantic. *Paleoceanography*. **22**, PA1219 (2007).
- O'Brien, C. L. et al. Cretaceous sea-surface temperature evolution: constraints from TEX<sub>86</sub> and planktonic foraminiferal oxygen isotopes. *Earth-Sci. Rev.* **172**, 224–247 (2017).
- Owens, J. D., Reinhard, C. T., Rohrsen, M., Love, G. D. & Lyons, T. W. Empirical links between trace metal cycling and marine microbial ecology during a large perturbation to Earth's carbon cycle. *Earth Planet. Sci. Lett.* **449**, 407–417 (2016).



7. Ostrander, C. M., Owens, J. D. & Nielsen, S. G. Constraining the rate of oceanic deoxygenation leading up to a Cretaceous Oceanic Anoxic Event (OAE-2; ~94 Ma). *Sci. Adv.* **3**, e1701020 (2017).
8. Scholle, P. A. & Arthur, M. A. Carbon isotope fluctuations in Cretaceous pelagic limestones: potential stratigraphic and petroleum exploration tool. *Am. Assoc. Pet. Geol. Bull.* **64**, 67–87 (1980).
9. Erbacher, J., Friedrich, O., Wilson, P. A., Birch, H. & Mutterlose, J. Stable organic carbon isotope stratigraphy across Oceanic Anoxic Event 2 of Demerara Rise, western tropical Atlantic. *Geochem. Geophys. Geosyst.* **6**, Q06010 (2005).
10. Owens, J. D., Lyons, T. W. & Lowery, C. M. Quantifying the missing sink for global organic carbon burial during a Cretaceous oceanic anoxic event. *Earth Planet. Sci. Lett.* **499**, 83–94 (2018).
11. Raven, M. R. et al. Paired organic matter and pyrite  $\delta^{34}\text{S}$  records reveal mechanisms of carbon, sulfur, and iron cycle disruption during Oceanic Anoxic Event 2. *Earth Planet. Sci. Lett.* **512**, 27–38 (2019).
12. Kuypers, M. M. M., Pancost, R. D., Nijenhuis, I. A. & Damsté, J. S. S. Enhanced productivity led to increased organic carbon burial in the euxinic North Atlantic basin during the late Cenomanian oceanic anoxic event. *Paleoceanography* **17**, 1051 (2002).
13. van Bentum, E. C. et al. Reconstruction of water column anoxia in the equatorial Atlantic during the Cenomanian-Turonian oceanic anoxic event using biomarker and trace metal proxies. *Palaeogeog. Palaeoclim. Palaeoecol.* **280**, 489–498 (2009).
14. Kuypers, M. M. M., van Breugel, Y., Schouten, S., Erba, E. & Damsté, J. S. S.  $\text{N}_2$ -fixing cyanobacteria supplied nutrient N for Cretaceous oceanic anoxic events. *Geology*. **32**, 853–856 (2004).
15. Higgins, M. B., Robinson, R. S., Husson, J. M., Carter, S. J. & Pearson, A. Dominant eukaryotic export production during ocean anoxic events reflects the importance of recycled  $\text{NH}_4^+$ . *Proc. Natl. Acad. Sci. USA* **109**, 2269–2274 (2012).
16. Junium, C. K., Freeman, K. H. & Arthur, M. A. Controls on the stratigraphic distribution and nitrogen isotopic composition of zinc, vanadyl and free base porphyrins through Oceanic Anoxic Event 2 at Demerara Rise. *Org. Geochem.* **80**, 60–71 (2015).
17. Junium, C. K., Keely, B. J., Freeman, K. H. & Arthur, M. A. Chlorins in mid-Cretaceous black shales of the Demerara Rise: the oldest known occurrence. *Org. Geochem.* **42**, 856–859 (2011).
18. Treibs, A. Chlorophyll and heme derivatives in organic mineral materials. *Angewandte Chem.* **49**, 682–686 (1936).
19. Damsté, J. S. S., Schouten, S., Hopmans, E. C., van Duijn, A. C. T. & Geenevasen, J. A. J. Crenarchaeol: the characteristic core glycerol dibiphytanyl glycerol tetraether membrane lipid of cosmopolitan pelagic crenarchaeota. *J. Lipid Res.* **43**, 1641–1651 (2002).
20. Zeng, Z. et al. GDGT cyclization proteins identify the dominant archaeal sources of tetraether lipids in the ocean. *Proc. Natl. Acad. Sci. USA* **116**, 22505–22511 (2019).
21. Liaaen-Jensen, S. Bacterial carotenoids. *Acta Chem. Scandinavica* **19**, 1025–1030 (1965).
22. Summons, R. E. & Powell, T. G. Identification of aryl isoprenoids in source rocks and crude oils: Biological markers for the green sulphur bacteria. *Geochim. Cosmochim. Acta.* **51**, 557–566 (1987).
23. Liu, X.-L., Zhu, C., Wakeham, S. G. & Hinrichs, K.-U. In situ production of branched glycerol dialkyl glycerol tetraethers in anoxic marine water columns. *Mar. Chem.* **166**, 1–8 (2014).
24. Grossi, V. et al. Mono- and dialkyl glycerol ether lipids in anaerobic bacteria: Biosynthetic insights from the mesophilic sulfate reducer *Desulfatibacillum alkenivorans* PF2803<sup>T</sup>. *Appl. Environ. Microbiol.* **81**, 3157–3168 (2015).
25. Bale, N. J. et al. New insights into the polar lipid composition of extremely halo(alkali)philic Euryarchaea from hypersaline lakes. *Front. Microbiol.* **10**, 377 (2019).
26. Coffinet, S. et al. Structural elucidation and environmental distributions of butanetriol and pentanetriol dialkyl glycerol tetraethers (BDGTs and PDGTs). *Biogeosciences* **17**, 217–330 (2020).
27. Du Vivier, A. D. C. et al. Marine  $^{187}\text{Os}/^{188}\text{Os}$  isotope stratigraphy reveals the interaction of volcanism and ocean circulation during Oceanic Anoxic Event 2. *Earth Planet. Sci. Lett.* **389**, 23–33 (2014).
28. Wilson, S. T. et al. Kilauea lava fuels phytoplankton bloom in the North Pacific Ocean. *Science.* **365**, 1040–1044 (2019).
29. Naafs, B. D. A. et al. Fundamentally different global marine nitrogen cycling in response to severe ocean deoxygenation. *Proc. Natl. Acad. Sci. USA* **116**, 24979–24984 (2019).
30. Lam, P. et al. Linking crenarchaeal and bacterial nitrification to anammox in the Black Sea. *Proc. Natl. Acad. Sci. USA* **104**, 7104–7109 (2007).
31. Junium, C. K., Meyers, S. R. & Arthur, M. A. Nitrogen cycle dynamics in the Late Cretaceous Greenhouse. *Earth Planet. Sci. Lett.* **481**, 404–411 (2018).
32. Owens, J. D. et al. Sulfur isotopes track the global extent and dynamics of euxinia during Cretaceous Oceanic Anoxic Event 2. *Proc. Natl. Acad. Sci. USA* **110**, 18407–18412 (2013).
33. Martin, E. E., MacLeod, K. G., Jiménez Berrococo, A. & Bourbon, E. Water mass circulation on Demerara Rise during the Late Cretaceous based on Nd isotopes. *Earth Planet. Sci. Lett.* **327–328**, 111–120 (2012).
34. Friedrich, O., Erbacher, J., Moriya, K., Wilson, P. A. & Kuhnert, H. Warm saline intermediate waters in the Cretaceous tropical Atlantic Ocean. *Nat. Geosci.* **1**, 453–457 (2008).
35. Trabucho Alexandre, J. et al. The mid-Cretaceous North Atlantic nutrient-trap: black shales and OAEs. *Paleoceanography* **25**, PA4201 (2010).
36. Kashiyama, Y. et al. Reconstruction of the biogeochemistry and ecology of photoautotrophs based on the nitrogen and carbon isotopic compositions of vanadyl porphyrins from Miocene siliceous sediments. *Biogeosciences* **5**, 797–816 (2008).
37. Kashiyama, Y. et al. Diazotrophic cyanobacteria as the major photoautotrophs during mid-Cretaceous oceanic anoxic events: Nitrogen and carbon isotopic evidence from sedimentary porphyrin. *Org. Geochem.* **39**, 532–549 (2008).
38. Zheng, X.-Y., Jenkyns, H. C., Gale, A. S., Ward, D. J. & Henderson, G. M. Changing ocean circulation and hydrothermal inputs during Ocean Anoxic Event 2 (Cenomanian-Turonian): evidence from Nd-isotopes in the European shelf sea. *Earth Planet. Sci. Lett.* **375**, 338–348 (2013).
39. Pedersen, T. F. & Calvert, S. E. Anoxia vs. productivity: what controls the formation of organic-carbon-rich sediments and sedimentary rocks? *Am. Assoc. Pet. Geol. Bull.* **74**, 454–466 (1990).
40. Karner, M. B., DeLong, E. F. & Karl, D. M. Archaeal dominance in the mesopelagic zone of the Pacific Ocean. *Nature.* **409**, 507–510 (2001).
41. Könneke, M. et al. Ammonia-oxidizing archaea use the most energy-efficient aerobic pathway for  $\text{CO}_2$  fixation. *Proc. Natl. Acad. Sci. USA* **111**, 8239–8244 (2014).
42. Steinacher, M. et al. Projected 21st century decrease in marine productivity: a multi-model analysis. *Biogeosciences* **7**, 979–1005 (2010).
43. Zhu, C. et al. Comprehensive glycerol ether lipid fingerprints through a novel reversed phase liquid chromatography-mass spectrometry protocol. *Organic Geochemistry* **65**, 53–62 (2013).
44. Liu, X.-L., Summons, R. E. & Hinrichs, K.-U. Extending the known range of glycerol ether lipids in the environment: structural assignments based on tandem mass spectral fragmentation patterns. *Rapid Comm. Mass. Spec* **26**, 2295–2302 (2012).
45. Zhu, C. et al. Identification and significance of unsaturated archaeal tetraether lipids in marine sediments. *Rapid Comm. Mass. Spec* **28**, 1144–1152 (2014).
46. DeRosa, M. et al. An asymmetric archaeobacterial diether lipid from alkaliphilic halophiles. *J. Gen. Microbiol.* **128**, 343–348 (1982).
47. Connock, G. T., Nguyen, T. X. & Philp, R. P. The development and extent of photic zone euxinia concomitant with Woodford Shale deposition. *Am. Assoc. Pet. Geol. Bull.* **102**, 959–986 (2018).

## Acknowledgements

We thank Dr. Kashiyama for providing standards of  $\text{C}_{30}$ -17-nor-DPEP and the IODP core repository for access to samples. J.D.O. acknowledges support from the Alfred P. Sloan Foundation, NASA Exobiology, and by the National High Magnetic Field Laboratory (Tallahassee, Florida). This work was supported by ACS PRF grant 61018-DNI2 (X.-L.L.), NSF Cooperative Agreement No. DMR1644779, and the State of Florida (J.D.O.).

## Author contributions

G.T.C. designed and performed the experiments, collected and analyzed the data, and wrote the paper. J.D.O. provided the samples and edited the paper. X.-L.L. designed the experiments, collected and analyzed the data, and edited the paper.

## Competing interests

The authors declare no competing interests.

## Additional information

**Supplementary information** The online version contains supplementary material available at <https://doi.org/10.1038/s43247-022-00466-x>.

**Correspondence** and requests for materials should be addressed to Gregory T. Connock.

**Peer review information** *Communications Earth & Environment* thanks thanks thanks Julio Sepulveda and the other, anonymous, reviewer(s) for their contribution to the peer review of this work. Primary Handling Editors: Mojtaba Fakhraee, Joe Aslin.

**Reprints and permission information** is available at <http://www.nature.com/reprints>

**Publisher's note** Springer Nature remains neutral with regard to jurisdictional claims in published maps and institutional affiliations.



**Open Access** This article is licensed under a Creative Commons Attribution 4.0 International License, which permits use, sharing, adaptation, distribution and reproduction in any medium or format, as long as you give appropriate credit to the original author(s) and the source, provide a link to the Creative Commons license, and indicate if changes were made. The images or other third party material in this article are included in the article's Creative Commons license, unless indicated otherwise in a credit line to the material. If material is not included in the article's Creative Commons license and your intended use is not permitted by statutory regulation or exceeds the permitted use, you will need to obtain permission directly from the copyright holder. To view a copy of this license, visit <http://creativecommons.org/licenses/by/4.0/>.

This is a U.S. Government work and not under copyright protection in the US; foreign copyright protection may apply 2022